Available online at www.sciencedirect.com
SCIENCE DIRECT
Thermochimica Acta 446 (2006) 41–54
thermochimica acta
www.elsevier.com/locate/tca

High-speed/high performance differential scanning calorimetry (HPer DSC): Temperature calibration in the heating and cooling mode and minimization of thermal lag

Geert Vanden Poel [a], Vincent B.F. Mathot [b,*]

[a] *DSM Research, P.O. Box 18, 6160 MD Geleen, The Netherlands*
[b] *SciTe, Ridder Vosstraat 6, 6162 AX Geleen, The Netherlands*

Available online 6 March 2006

Abstract

The temperature calibration of high performance DSC in the heating and cooling mode is discussed. Several primary and secondary calibration standards are studied at different sample masses – from 0.4 μg to 10 mg – and various heating and cooling rates – from 1 to 500 °C/min and from 1 to 300 °C/min, respectively. The experimental onset and peak temperatures of Indium with different sample masses are measured at different heating rates and the two related correction factors are presented. The symmetry of the HPer DSC with respect to the cooling and the heating modes is checked and found to be good. The liquid crystals M24, HP-53 and BCH-52, being substances with no or very small supercoolings, are recommended as secondary standards for temperature calibration in both the cooling and heating mode. In order to verify whether the proposed correction factors of Indium can also be used in the cooling mode, the melting behavior of Indium and the phase transition temperatures of the secondary standards obtained in heating are compared, and it turns out that the latter are usable as well. Finally, recommendations for both an extensive temperature calibration and a rather quick calibration procedure of scanning calorimeters in the heating and the cooling mode for various sample masses and various rates are given. The calibration procedure developed for HPer DSC facilitates making the right choices to minimize the thermal lag with respect to the sample mass and scan rates at the start of the measurement, instead of just making corrections afterwards.

Keywords: High performance differential scanning calorimeter; HPer DSC; HyperDSC; Cooling rate; Heating rate; Liquid crystal; Thermal lag; Calibrants

1. Introduction

A relatively new high-speed calorimetry technology, high performance DSC (HPer DSC; see http://www.scite.nl), has recently been discussed for practical use and since then marketed by PerkinElmer under the name HyperDSC™, see http://www.hyperdsc.com. Mathot and co-workers published the detailed characteristics and use of this new mode of measurement, which represents a major step forward in high-speed calorimetry, as compared to standard DSC [1]. Controlled and constant scan rates of hundreds of degrees per minute and combinations thereof both in the cooling and heating mode are possible. Heats of transition, heat capacities, temperature-dependent crystallinities, etc. can be established at the extreme rates applied. The short measuring times also provide the high throughput needed in combinatorial chemistry.

Application fields concerning HPer DSC are situated in the study of the kinetics and metastability of macromolecular and pharmaceutical systems, particularly in the analysis of rate-dependent phenomena at real temperature–time conditions. HPer DSC is very much suited to investigate kinetics of processes like crystallization, cold crystallization, recrystallization, annealing, and solid-state transformations in polymers, pharmaceuticals and liquid crystals. (Sub)milligram amounts of material can be investigated at very high, controlled cooling and heating rates of hundreds of degrees per minute, which facilitates the analysis of films, expensive and extraordinary products, inhomogeneities in materials, etc. High cooling rates need to be applied to simulate processing conditions like in film blow molding, injection molding and extrusion. It turns out that for some processing techniques the cooling rate can be mimicked by HPer DSC. Measurements concerning metastability and kinetics are

* Corresponding author. Tel.: +31 6 14849332; fax: +31 84 8346102.
E-mail addresses: geert.poel-vanden@dsm.com (G. Vanden Poel), vincent.mathot@scite.nl (V.B.F. Mathot).

0040-6031/$ – see front matter © 2006 Elsevier B.V. All rights reserved.
doi:10.1016/j.tca.2006.02.022

also necessary to (re)connect heating behavior with cooling history.

This article discusses the fundamental requirements for a universally applicable and unified correct temperature calibration in the heating and cooling mode of high performance differential scanning calorimeters. High-speed calorimeters need a new approach for calibration, in order to deal with different high heating and cooling rates and the adjustment needed with respect to the sample masses. An important additional goal is to provide procedures to optimize experimental conditions – especially to minimize thermal lag – before starting the measurement.

Calibration has to be performed to correct for the thermal lag: increasing *sample mass*/*size* increases the thermal lag of sample temperature versus sensor temperature and in addition gives risk to temperature gradients within the sample resulting in peak broadening, while increasing the *heating and cooling rates* increases the thermal lag of the sensor temperature with respect to the furnace temperature. To characterize the thermal lags in the system and sample, it is useful to differentiate between an outside thermal resistance: R_o, and a thermal resistance within the sample: R_s. The outside thermal resistance consists of a thermal resistance related to the instrument, R_i, and a thermal contact resistance between the container and the instrument, R_c. The total thermal resistance, R, is defined as the sum of R_o and R_s. The temperature calibration of HPer DSC will be done in subsequent steps: first a regular calibration will be performed with primary standards, and then a calibration matrix with respect to scan rate and sample mass will be developed in the heating mode. The symmetry of the HPer DSC furnaces will be checked using secondary standards, by working both in the cooling and heating mode. Finally, the results of the secondary calibrants obtained in heating are compared to the melting characteristics of Indium.

2. Experimental

Measurements were performed with a modified PerkinElmer Pyris 1 calorimeter having software version 7.0. This power-compensation DSC was selected to be used as an HPer DSC because its furnace has low mass and small dimensions, ensuring a much faster heat transfer than in the existing commercial heat-flux calorimeters. The small gap between the furnace and the aluminum cooling system, which is even reduced by guard ring inserts, promotes effective cooling. The HPer DSC was cooled with a cryofill system, which represents a very effective heat sink. Special attention was paid to the avoidance of water uptake by the gas tubes in the instrument, to the cooling of the instrument electronics, and to the prevention of water vapor condensation. To prevent moisture on the cooling system, which was cooled to a temperature of −178 °C, a completely air-sealed glove box was installed on top of the HPer DSC. Dry nitrogen gas was used to purge the glove box. The choice of the gas atmosphere surrounding the reference and sample furnaces depends on the specific system and on the temperature range to be studied. In most cases, a mixture of 10% helium and 90% neon is suited for a combination of a temperature range of −176 to 585 °C and typical controlled, constant scan rates as high as 450 °C/min for the heating mode and 250 °C/min for the cooling mode (within a limited temperature range). Both of these inert gases do not condense under cooling by liquid nitrogen. With regard to the heat conduction around the reference and sample furnaces, the mixture offers a useful compromise [2]. Pure helium is in itself an excellent heat conductor and can be used to maximize heat transfer, which offers benefits in measurements down to low (subambient) temperatures. However, when it comes to reaching high temperatures, the furnace will be a limiting factor, because the helium causes too much heat loss so that the furnace can no longer control the temperature beyond the ceiling level of about 200 °C. Neon [3] conducts heat less well (but better than nitrogen), and makes it possible to control the temperature in the higher ranges. It is even possible to use standard nitrogen as long as it is prevented from condensing as a result of the presence of liquid nitrogen cooling. Default isothermal waiting times between runs amount to 5 min, although this time can be shortened to, e.g. 1 min. To promote optimal thermal contact between the sample and the sensor, a 15 μm thin aluminum foil of approximately 0.5 cm × 1 cm is normally used to wrap the sample, instead of using a pan as sample container. On the reference container an aluminum foil of the same dimensions is placed. If a lower accuracy is acceptable, it is also possible to use pans of aluminum.

3. Temperature calibration

A correct way to perform temperature calibration for the HPer DSC starts with a regular calibration over a wide temperature range using primary standards, which are selected on the basis of their phase transition temperatures situated in the temperature range of interest. Thereafter, a calibration matrix is set-up for different heating rates and various sample masses on the basis of one primary standard. Once the calibration in the heating mode has been performed, the symmetry of the instrument's behavior with respect to heating and cooling is validated. If an asymmetry is found a separate calibration for the cooling mode is inevitable. This calibration procedure looks elaborated but is inevitable when using high scan rates and various sample masses. Moreover, the power compensated DSC used has the advantage of a considerably light furnace with small dimensions in comparison with most commercial heat-flux DSC's, which reduces the thermal lag by fast heat transfer. Up to now, no high cooling rates – as compared with those attained by the power compensated DSC used – can be achieved using a commercial heat-flux DSC.

Adamantane, Gallium, Benzophenon, Indium and Tin have been used as primary standards to calibrate the power-compensation differential scanning calorimeter (PerkinElmer Pyris 1), which was adapted to perform high performance DSC measurements [1] in the heating mode for the temperature range of −150 to 350 °C. The sample masses of these calibration substances were chosen between 0.99 and 1.01 mg with an applied heating rate, S_h, of 10 °C/min. In practice, samples of about 1 mg are easily to handle during preparation concerning HPer DSC experiments and their signal-noise ratio is high enough to obtain proper results even for slow cooling and heating rates.

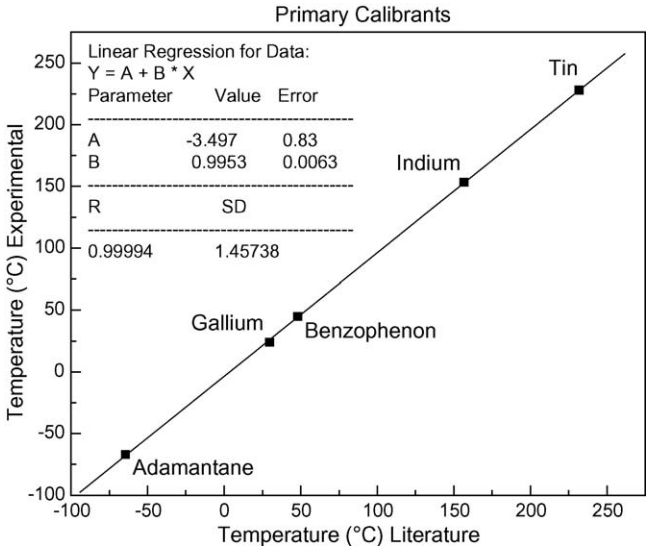

Fig. 1. Temperature calibration of a power-compensation differential scanning calorimeter in the heating mode.

Fig. 1 represents the calibration curve while the phase transition temperatures of the calibration substances are listed in Table 1 [4–16]. The extrapolated onset T_{EO} or the peak extremum temperature T_P is determined for all peaks obtained. The temperature of the intersection of the auxiliary line through the leading edge of the peak with the linearly (from the low-temperature side of the peak) extrapolated baseline is defined as the extrapolated onset temperature. The extrapolated onset and not the 'real' onset (the temperature where the DSC curve deviates from the baseline) is used for calibration due to the following reasons. First of all, it is arbitrary to determine accurate the 'real' onset value for heating scans obtained using high rates (>50 °C/min). Secondly, the extrapolated onset refers in a better way the start of the melting behavior of the bulk of the material. The temperature of the extremum (maximum heat flow rate in heating, minimum heat flow rate in cooling) of the DSC curve is called the peak extremum temperature or short: peak temperature. The linearity of the calibration curve (Fig. 1) suggests that only one standard should do to have the power-compensation DSC calibrated over the whole temperature range, e.g. by using Indium. Nevertheless, the authors advise to use at least three standards (like for instance Adamantane, Indium and Tin), which should cover the temperature range of interest in order to arrive at an accurate calibration, because the extensive temperature calibration concerning various sample masses and different scan rates relies on it. Later on, when using the HPer DSC for regular high-speed measurements, a simple temperature check of Indium is sufficient to verify whether or not the calibration is still valid.

Illers [17] tried to correct for thermal lag, which causes a shift of the melting peak extremum by ΔT to higher temperature with respect to the extrapolated onset temperature. He studied the influence of heating rate at constant sample mass on ΔT. A linear relation was found for ΔT as a function of the square root of the heating rate (up to 36 °C/min):

$$\Delta T = A(BS_h)^{1/2} \quad (1a)$$

with S_h = the heating rate (°C/min);
$\Delta T = T_{Peak} - T_{Extrapolated\ Onset}$ (°C); $A = RC_s$ (min); R is the total thermal resistance (the sum of R_i, the thermal resistance of the instrument; R_c, the thermal contact resistance between the container and the instrument and R_s, thermal resistance within the sample) in °C min/J and C_s is the heat capacity of the sample and sample container (sample plus aluminum foil) in J/°C. $B = 2\Delta H_m/(RC_s^2)$ (°C/min); ΔH_m is the enthalpy of melting in J.

(1a) can be written as

$$\Delta T = \sqrt{2R\Delta H_m S_h} \quad (1b)$$

if $R_s \ll R_o = R_i + R_c$, $R = R_o \cong$ constant and (1b) becomes:

$$\Delta T \propto \sqrt{mS_h} \quad (1c)$$

Table 1
Substances recommended for temperature calibration in the cooling and heating mode

Substance	Evaluation T_{EO} or T_P	Type of transition	Phase transition temperature, T_{trs}		Supercooling (°C)	Literature
			(°C)	(K)		
Adamantane	T_{EO}	Solid–solid	−64.53	208.62	<1	[5–7,10]
Gallium[a]	T_{EO}	Solid–liquid	29.76	302.91	25	[5,11,14,16]
Benzophenon[b]	T_{EO}	Solid–liquid	48.1	321.25	–	
M24	T_P	Smectic–nematic	67.1	340.25	<0.2	[4,5]
HP-53	T_P	Smectic–nematic	120.5	393.65	<0.2	[4,5]
4,4′-Azoxyanisole	T_{EO}	Liquid crystal–isotropic crystal	135.85	409	[c]	[8,9,16]
Indium	T_{EO}	Solid–liquid	156.6	429.75	<2	[5,11,15]
BCH-52	T_P	Nematic–liquid	164.8	437.95	<0.2	[4,5]
Sn	T_{EO}	Solid–liquid	231.93	506.08	20	[5,12,13]

[a] Gallium very easily reacts with aluminum, which is usually used as crucible material. To avoid alloy formation with potential subsequent destruction of calorimeter components, it is therefore necessary to proceed very carefully and with great attention. It is advised to use only fresh samples, to examine the crucible bottom for cracks in the aluminum oxide layer, and to immediately cut short a series of experiments as soon as during successive experiments an increase of the peak width or a decrease of the peak area is observed. The authors do not accept any responsibility for any damage!

[b] Benzophenon will sublimate above its melting temperature, it is therefore advised to use it only once. No crystallization can be observed during cooling.

[c] It is rather difficult to determine a supercooling degree for the 4,4′-Azoxyanisole used because two melting and two crystallization peaks are observed for the applied heating and cooling rates of 1 and 5 °C/min as can be seen in Fig. 3.

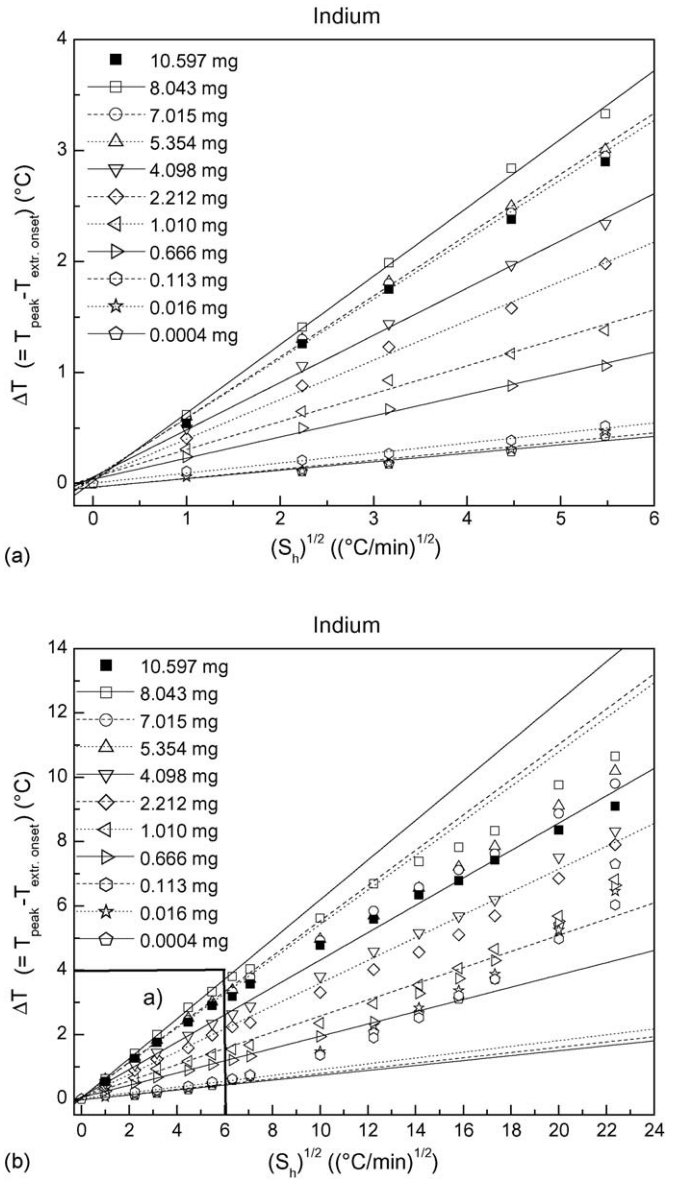

Fig. 2. ΔT (melting peak temperature – extrapolated onset) as function of the square root of the heating rate, S_h, according to Illers. For low S_h (up to 36 °C/min) linearity is preserved for various masses of Indium (magnified curve), see (a). Higher S_h shows large deviations from this linear behavior, see (b).

A rule of the thumb of the calibration for a HPer DSC concerning high scan rates, both in cooling and in heating has been mentioned by Pijpers et al. [1] based on (1c): in order to minimize thermal gradients within a sample in the case of HPer DSC; if the scan rate is increased by a factor of x, the sample mass was suggested to be reduced by the same factor x. In addition, an aluminum foil was recommended for use, instead of a pan as a sample container, which provides a drastically improved way of heat transfer. Fig. 2a confirms the result found by Illers. However this linearity cannot be extended to higher heating rates (up to 500 °C/min) as is shown in Fig. 2b. The trend with respect to the deviations from linear behavior appears to be dependent on sample mass: for low sample mass (<1 mg) ΔT increases more than in the linear case with $S_h^{1/2}$; for high sample masses (>1 mg) ΔT increases less than in the linear case. In Fig. 3, the increase in thermal lag can be seen from the extrapolated onset and the peak temperatures for various heating and cooling rates – S_h and S_c, respectively – and various masses for 4,4′-Azoxyanisole and Adamantane samples. 4,4′-Azoxyanisole shows two transitions on heating at 10 °C/min: (1) melting (solid–liquid crystal) at 115.85 °C and (2) a liquid crystal–isotropic liquid transition at 135.85 °C, which latter is shown in Fig. 3a and b. The first transition has a very large supercooling effect, but the second transition is completely reversible and can therefore be used for DSC calibration during cooling. Fig. 3 represents the HPer DSC curves of the 4,4′-Azoxyanisole liquid crystal–isotropic liquid transition for S_h going from 1 up to 200 °C/min and the HPer DSC curves of the isotropic liquid–liquid crystal transition of 4,4′-Azoxyanisole for S_c going from 1 up to 250 °C/min. Due to the overlap of the solid–liquid crystal transition with the liquid crystal–isotropic liquid at high heating rates ($S_h > 200$ °C/min) and the observation of a double peak behavior in the present study (which cause is unknown) at low heating and cooling rates, this compound is not an ideal substance for temperature calibration of HPer DSC. Adamantane can be used for the calibration of HPer DSC both in the cooling and heating mode because it has a fast reversible solid–solid transition at −64.53 °C with almost no supercooling. The extrapolated onset and peak temperature values of Adamantane for two sample masses (0.663 and 1.598 mg) are plotted in Fig. 3c. The increase of the peak temperature with the heating rate is more pronounced than the increase of the extrapolated onset. In the same way, the peak temperature decrease is more pronounced than that of the extrapolated onset in the cooling mode for relatively low cooling rates ($S_c < 100$ °C/min). For higher cooling rates ($S_c \geq 100$ °C/min), the peak and extrapolated onset values remain constant with varying cooling rates, indicating that the instrumental limits for fast cooling at these particular low temperatures are reached with the cooling set-up used. Other clear examples of thermal lag resulting from sample mass and heating rate as reflected by the extrapolated onset and the peak temperatures are shown in Fig. 4 for the primary standard, Indium. The results discussed illustrate the need for a more extended temperature calibration of HPer DSC's. In general, it is wise to search for other standards for HPer DSC calibration during cooling as will be discussed further on.

3.1. Temperature calibration in the heating mode

Subsequent to the calibration of the HPer DSC using at least three primary standards, which should cover the temperature range of interest, a calibration matrix for scan rate and sample mass should be constructed for all heating rates applied. Primary and/or secondary standards can be used to develop this calibration matrix. In this article Indium is chosen because of its practical use. Several samples of Indium are weighed in for masses between 0.1 and 10 mg and the extrapolated onset and peak temperatures are measured in order to construct the usable sample mass/heating rate window for the respective HPer DSC instrument (Fig. 4, see also Fig. 2 for lower sample masses down to 0.4 μg). The extrapolated onset of an Indium sam-

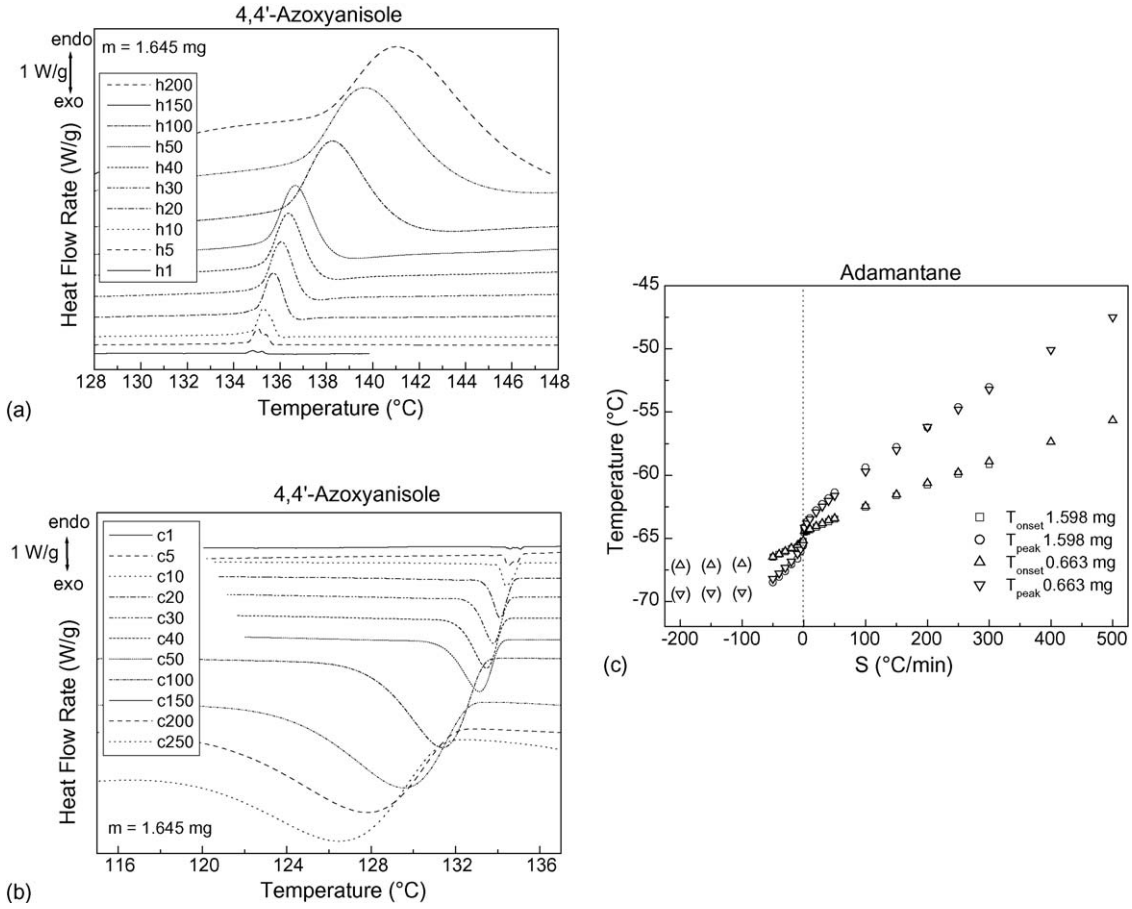

Fig. 3. (a) HPer DSC heating curves of the transition liquid crystal–isotropic liquid of 4,4′-Azoxyanisole for S_h going from 1 up to 200 °C/min, (b) HPer DSC cooling curves of the transition isotropic liquid–liquid crystal of 4,4′-Azoxyanisole for S_c going from 1 up to 250 °C/min and (c) the extrapolated onset and peak temperature values of Adamantane in both cooling and heating for two sample masses (0.663 and 1.598 mg). The data points between brackets show the impossibility of reaching the higher cooling rates at these particular low temperatures.

ple of 0.113 mg measured at a heating rate of 500 °C/min is 4.1 °C higher than that of the same Indium sample but measured at 1 °C/min, while the difference for the peak temperatures is 10.1 °C. For an Indium sample of 8.043 mg the differences between heating rates of 1 and 500 °C/min are, respectively, 9.6 and 19.6 °C for the extrapolated onset and the peak temperatures. The temperature difference between the extrapolated onsets of two Indium samples of 0.113 and 8.043 mg is 0 and 5.5 °C for, respectively, heating rates of 1 and 500 °C/min. In an identical way peak temperature differences of 0.5 and 10.1 °C are measured for these samples at the same heating rates. This means that decreasing the sample mass reduces indeed (drastically) the thermal lag but it is almost impossible to compensate fully its increase due to increasing scan rate. Examples of HPer DSC curves of Indium melting for two sample masses, 0.113 and 5.354 mg, and different heating rates, S_h from 1 to 500 °C/min, are shown in Fig. 5. A description of a melting peak is depicted in an idealized form, i.e. the inserted picture in Fig. 5. The slope of the low-temperature side of the Indium curve is proportional to the reciprocal thermal resistance R. As defined before, R equals the thermal resistance related to the outside thermal resistance: R_o, plus the thermal resistance within the sample: R_s. It is remarkable that the slope of the low-temperature side of Indium in Fig. 5a decreases with increasing heating rate, while that of Indium in Fig. 5b remains constant at first sight. These observations can be explained according to Fig. 6, which represents the experimental values of ΔT ($=T_P - T_{EO}$) as a function of the square root of the sample mass multiplied with the heating rate. When the sample mass varies between 100 μg and 5 mg, and the heating rate is lower than 36 °C/min, a linear behavior of ΔT is found, which is described by the equation of Illers (Formula 1c, see Fig. 2a). These samples with intermediate masses (100 μg < m < 5 mg) present an upturn of the ΔT for relatively high heating rates. Once the sample mass drops down below 100 μg, R_s becomes negligible and R equals $R_o = R_i + R_c$, which means that the thermal resistance should be mainly dependent on the heating rate. A steep slope for 0.0004 and 0.016 mg of Indium can be observed in Fig. 6, reflecting the thermal resistance of the instrument and the thermal contact resistance between the container and the instrument. Hence, this means in practice that with increasing scan rate the slope of the low-temperature side of the melting curve changes from high to low values (see Fig. 5a) for a low sample mass, e.g. lower than approximately 5 mg. In this particular case, the contribution of R_s to the total thermal resis-

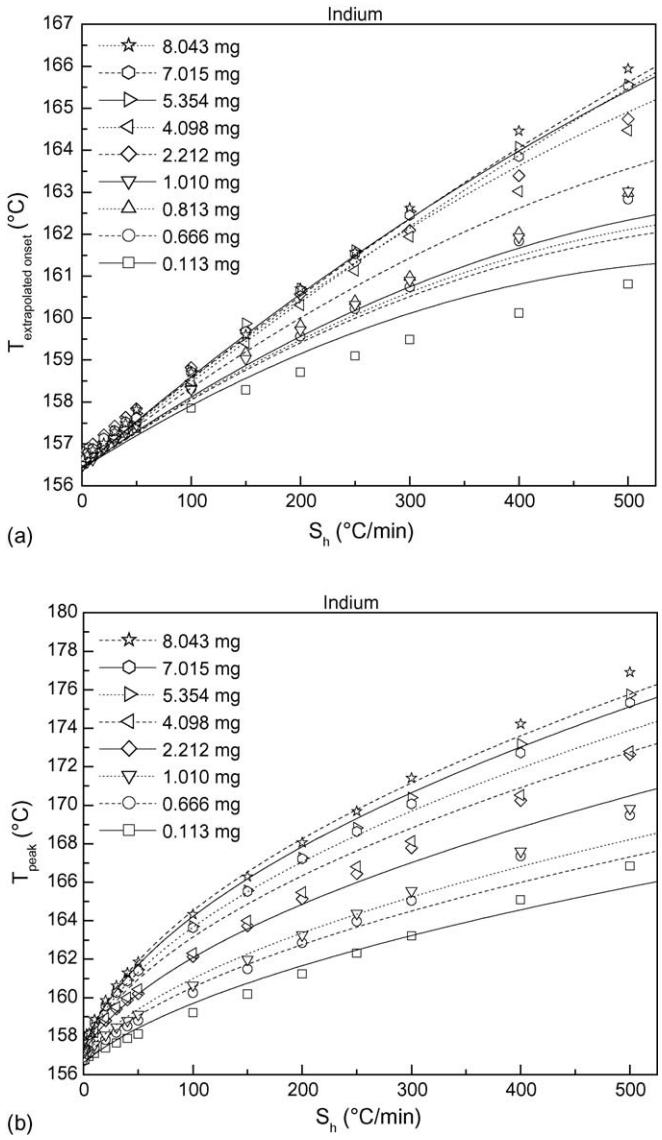

Fig. 4. The influence of the sample mass on (a) the extrapolated onset and (b) the peak melting temperatures of Indium as a function of the heating rate, S_h. The lines represent the fits using the multivariate linear regression-analysis method.

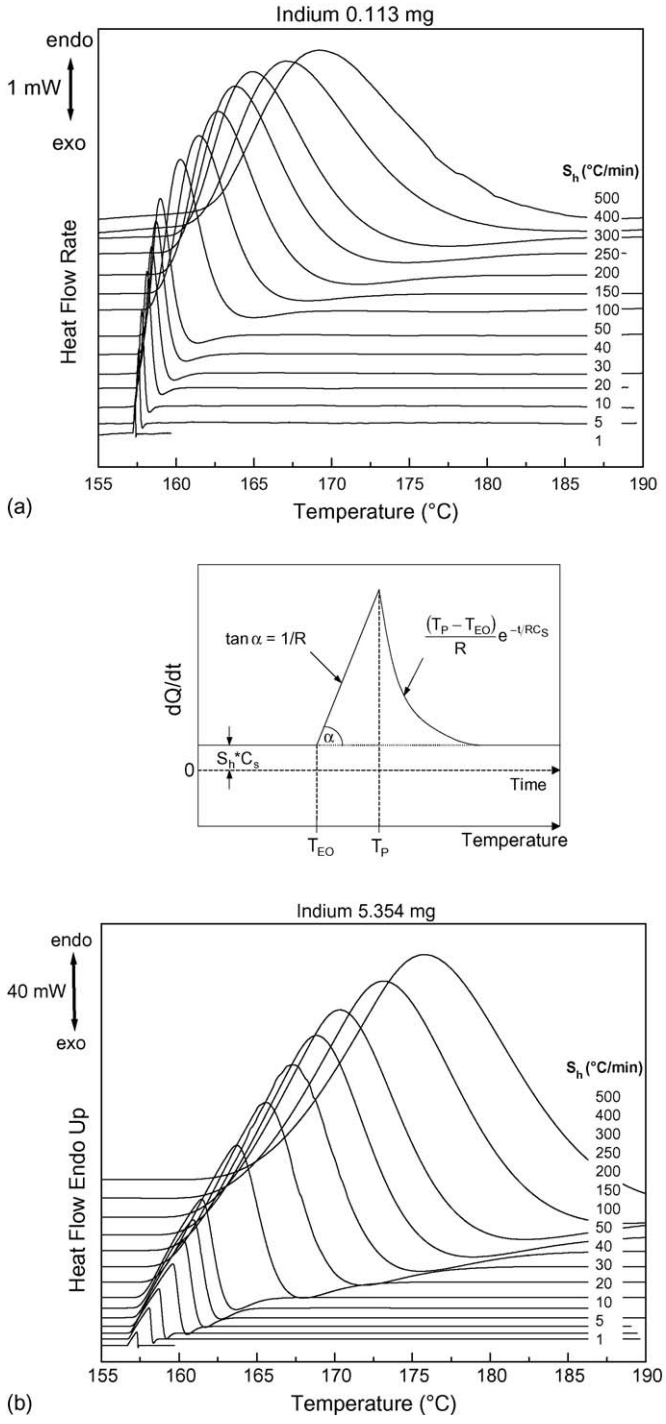

Fig. 5. HPer DSC heating curves of Indium melting, for samples with (a) a mass of 0.113 mg and (b) 5.354 mg, at various heating rates (S_h from 1 to 500 °C/min). α: angle, β: heating rate, R: thermal resistance, t: time, T_P: peak temperature, T_{EO}: extrapolated onset and C_s: heat capacity of the sample. Inert: idealized melting curve of a calibration standard.

tance is much smaller than that of $R_o = R_i + R_c$. The dimensions of the container and the mode of contact – determining R_c – have been kept identical during all measurements. As a result, a high heating rate induces a large thermal lag, because the thermal resistance of the furnace and the contact resistance between container and the instrument may be mainly dependent on the heating rate. Once the sample mass is high enough, e.g. around 5 mg, the low-temperature side of the melting curve remains approximately independent of the heating rate (Fig. 5b), which means that the thermal resistance of the sample has a reasonable contribution to the total thermal resistance, R.

Another way to explain the results presented in Figs. 5 and 6 is to use the extended formula of Illers [17] (Eq. (2)). Eq. (2) can be rewritten into Eq. (3), which can be corrected for the heat capacity of relevance, outside the sample, C_o (Eq. (4)). The dependencies for the small sample masses in Fig. 6 can be explained by simplifying Eq. (4) to: $\Delta T \cong (2\Delta H_m R S_h)^{1/2} + S_h R C_o$. It is clear that in Fig. 6 the increase in slope of the experimental values of ΔT as a function of $(mS_h)^{1/2}$ is related to the additional term $S_h R C_o$. For large sample masses and heating rates, the slope of the experimental values of ΔT as a function of $(mS_h)^{1/2}$ is related to the term $Rc_s\{(1 + (2\Delta h_m / R m_s c_s^2 S_h))^{1/2} - 1\} + RC_o/m_s$, where $\Delta h_m = \Delta H_m/m_s$ and $c_s = C_s/m_s$ are the specific enthalpy

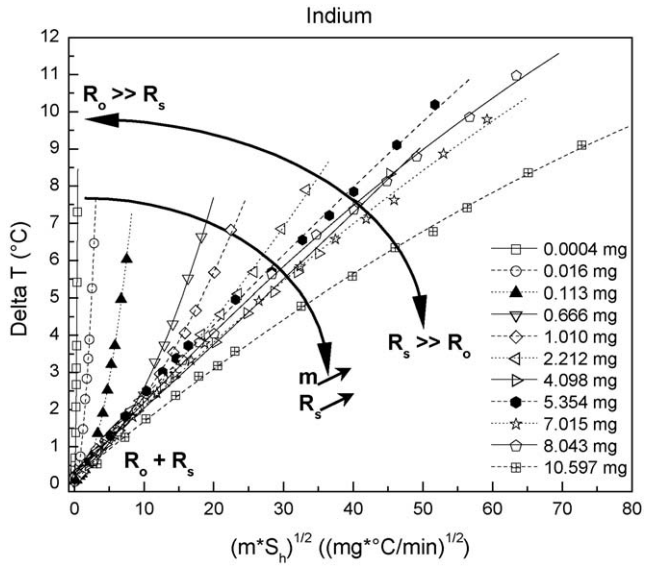

Fig. 6. The experimental values of ΔT ($=T_P - T_{EO}$) of Indium as a function of the square root of the sample mass multiplied with the heating rate. R: thermal resistance, R_o: the outside thermal resistance, R_s: thermal resistance within the sample and m: sample mass.

and the specific heat capacity of the sample, respectively. When the sample mass and heating rate increase to the limiting case: $m_s S_h \gg 2\Delta h_m / R c_s^2$, the slope in Fig. 6 tends to RC_o/m_s.

Fig. 7 shows the HPer DSC curves of Indium melting with masses of 0.016, 1.010, 5.354 and 8.043 mg at a heating rate of 150 °C/min. These heat flow rate curves are multiplied with 502.69, 7.96, 1.50 and 1, respectively, to compare with the heat flow rate curve of the 8.043 mg Indium sample. In this way, it can be clearly seen that the extrapolated onset of Indium shifts to higher values with increasing sample mass for one particular heating rate. The peak temperature shows an even larger shift with increasing sample mass, as is already mentioned above.

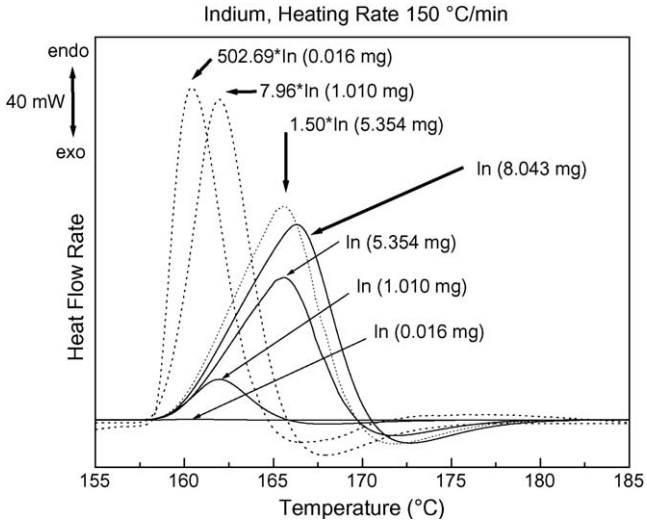

Fig. 7. HPer DSC heating curves of Indium melting for four different masses at $S_h = 150$ °C/min (lines). The dotted curves represent the 0.016, 1.010 and 5.354 mg Indium curves multiplied by their respective factors to equal the 8.043 mg Indium curve.

The measured melting enthalpies (Δh_m) of the Indium samples with various masses are presented in Table 2 as a function of the heating rate. The enthalpy values do not diverge too much with the reference value ($\Delta h_m^\circ = 28.45$ J/g). Lower enthalpy values ($\Delta h \leq 28$ J/g) are measured for low sample masses of Indium (0.113 and 0.666 mg) when the heating rate is below 100 °C/min (dark shaded area in Table 2). Nevertheless, these enthalpy values are accurate enough to be used; the maximal deviation is only within a 3% margin of error. A systematic error is made for all Indium samples during the calculation of the melting enthalpy for high heating rates ($\Delta h \geq 28$ J/g for $S_h \geq 100$ °C/min), which has a maximum margin of error up to 8% (light shaded area in Table 2). As can be seen in Fig. 5, the peaks are much more broadened at high heating rates, which explain the rather 'high' deviation of the Δh_m values in comparison with the reference melting enthalpy. No values are presented for heating rates above 300 °C/min because the peak broadening becomes that large that heat capacity measurements are needed for a decent calculation of the melting enthalpy. The fact that in case of Indium the heat capacities at temperatures below and above the melting temperature are almost identical, backs a simple straight line drawing of the baseline. Almost all melting curves show an exothermal heat flow rate signal just at the high temperature side of the endothermic peak, which has an instrumental origin and has to be taken into account while calculating the melting enthalpy by subtracting its area from the endothermic peak area. The boundaries for the calculation of the enthalpy area are chosen as follows: at the low-temperature side, on the baseline before the onset of the melting and at the high temperature side, above the exotherm where the DSC curve reaches again the baseline.

It is worthwhile to mention that the HPer DSC can measure – at least from typically 1 to 100 °C/min – samples with very low masses, i.e. Indium samples with masses down to 0.0001 mg, i.e. 100 ng. These kinds of samples need an additional preparation step because balances capable to weigh sample masses lower than 0.001 mg in a precise way are rare. Indium slices of predefined dimensions – in the order of 200 μm × 200 μm × 0.35 μm – were cut using a microtome, Leica RM 2165, at room temperature, and the mass of the slice was calculated using the density of Indium of 7.31 g/cm^3 at 27 °C. The exact sample mass is also verified and/or adjusted by the melting enthalpy obtained via the HPer DSC measurement.

Experimental results (see Fig. 2b) indicate a limit to the lowering of the sample mass used in order to decrease the thermal lag using a primary temperature standard at higher heating rates. No differences are found concerning ΔT within the margin of error for samples with masses varying from 0.0004 to 0.113 mg. Thus, despite the lowering of the sample mass there seems also to be no improvement at high heating rates: most probably the limits of the apparatus are encountered. Therefore, it is of no use to reduce the sample mass below 0.1 mg to minimize the thermal lag problem caused by high heating rates. Nevertheless, one is capable to measure samples of such a low mass and this is also very beneficial for many applications like for instance the thermal study of foils, coatings, nanomaterials, contaminations, minute amounts from fractionations, etc. Increasing the mass of

Table 2
The melting enthalpies of Indium, $\Delta h_m^\circ = 28.45\,J/g$, with various masses as a function of the heating rate

S_h (°C/min)	Measured melting enthalpies of Indium Δh_m (J/g)								
	Sample mass (mg)								
	0.113	0.666	0.813	1.01	2.212	4.098	5.354	7.015	8.043
1	27.84	28.06	28.31	27.98	28.10	28.33	28.26	28.13	28.18
5	27.61	27.96	28.34	28.51	28.15	28.34	28.22	28.24	28.22
10	27.68	28.06	28.41	28.51	28.18	28.35	28.27	28.31	28.27
20	27.56	28.36	28.47	28.54	28.28	28.48	28.28	28.35	28.35
30	28.07	28.35	28.65	28.64	28.39	28.61	28.44	28.46	28.4
40	27.81	28.41	28.49	28.57	28.41	28.66	28.49	28.44	28.5
50	27.66	28.58	28.81	28.71	28.41	28.71	28.64	28.62	28.55
100	29.01	28.81	29.26	29.18	28.91	29	28.87	28.93	28.88
150	29.69	29.24	29.44	29.77	29.42	29.45	29	29.4	29.18
200	29.35	30.65	29.83	30.41	30.03	29.87	29.46	29.75	29.43
250	29.5	30.77	29.41	30.07	29.55	29.14	29.33	29.33	29.2
300	28.79	30.54	28.23	29.8	28.76	28.97	28.92	28.93	29.01

the Indium sample from 0.1 up to 8 mg induces an increasing thermal lag. From Fig. 2b it is not clear whether an upper limit exists for ΔT. The extrapolated onsets of the 10.597 mg Indium sample coincide with those of the 5.354, 7.015 and 8.043 mg Indium samples, indicating an upper limit. The peak temperatures of the 10.597 mg Indium sample are somewhat lower than the 8.043 mg Indium sample for high heating rates and coincide with those of the 5.354 and 7.015 mg Indium samples. Therefore, the supposition can be made that it is not recommended to use samples with masses above 5 mg for high heating rates.

The formula used earlier, see (1a)–(1c) and Fig. 2, describing a linear relation between ΔT and $(S_h)^{1/2}$ for a sample having a mass m, was in fact a simplification of the following formula [17]:

$$\Delta T = A\{(BS_h + S_h^2)^{1/2} - S_h\} \quad (2)$$

with S_h = the heating rate (°C/min);
$\Delta T = T_{Peak} - T_{Extrapolated\ Onset}$ (°C); $A = RC_s$ (min); R is the total thermal resistance (the sum of R_i, the thermal resistance of the instrument; R_c, the thermal contact resistance between the container and the instrument and R_s, the thermal resistance within the sample) in °C min/J and C_s is the heat capacity of the sample in J/°C; $B = 2\Delta H_m/(RC_s^2)$ (°C/min); ΔH_m is the enthalpy of melting in J.

Eq. (2) can be rewritten into:

$$\Delta T = S_h RC_s \left\{ \left(1 + \frac{2\Delta H_m}{RC_s^2 S_h} \right)^{1/2} - 1 \right\} \quad (3)$$

Eq. (3) can be corrected for the heat capacity of relevance, outside the sample, C_o:

$$\Delta T = S_h RC_s \left\{ \left(1 + \frac{2\Delta H_m}{RC_s^2 S_h} \right)^{1/2} - 1 \right\} + S_h RC_o \quad (4)$$

The formula of Eq. (2) has been checked whether or not it could fit the experimental results also for high heating rates, see Fig. 8. The parameters A and B tend to depend strongly on the sample mass, m, and in a non-linear way. It can be noticed that the formula fits the experimental data of ΔT values well for samples having a mass above 1 mg in combination with applied heating rates up to 300 °C/min. At higher heating rates systematic deviations occur: the experimental data points have higher ΔT values than the lines representing the fittings. Samples with masses below 1 mg deviate strongly, especially at heating rates of 100 °C/min and higher. The reason for these disappointing results remains unclear at the moment. Exactly the combination of low sample mass and high heating rate, is extremely interesting for HPer DSC experiments. The deviations in this area become so distinctive for samples of masses beneath 0.666 mg that one may conclude that the formula is of no use for such samples. Therefore, to arrive at a decent fitting of the experimental data another approach has been chosen.

The following procedure has been set-up to develop a calibration matrix with respect to sample mass and heating rate. The extrapolated onset and the peak temperature values of Indium

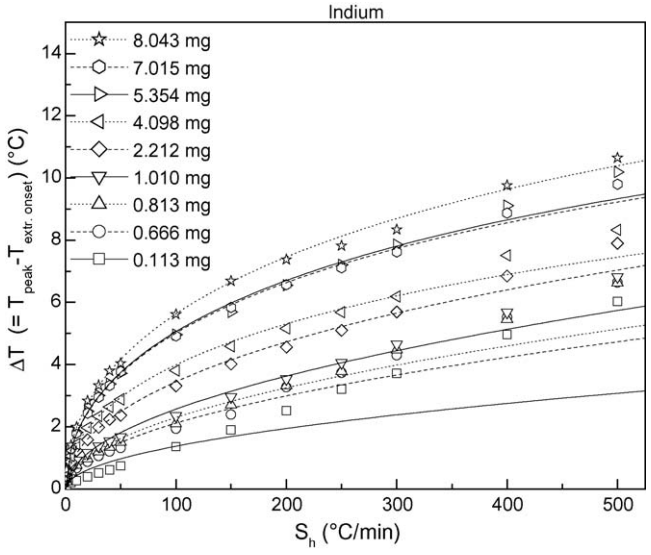

Fig. 8. ΔT values (melting peak – extrapolated onset temperatures) of Indium as function of the heating rate, S_h. The lines represent the fits using formula (2) by Illers.

with various sample masses (0.113–8.043 mg) and different heating rates (1–500 °C/min) are fitted with a function with sample mass and heating rate being the parameters, using the multivariate linear regression-analysis method. An experimental error of 0.1 °C for extrapolated onset and peak temperatures measured from 1 up to 50 °C/min and an experimental error of 1 °C for extrapolated onset and peak temperatures measured at 100 °C/min and higher have been taken into account. The fitting designs used are black box models, which pretend only to reproduce the measurements within the experimental error. Because these models do not have any physical significance, extrapolation outside the parameters range is not advisable. The mathematical fitting procedures induce two formulas: one concerning the extrapolated onset as a function of sample mass and heating rate, and another concerning the peak temperature as a function of sample mass and heating rate. As a result two correction factors originate on the basis of the reference values, 156.6 °C for the extrapolated onset and 157.6 °C for the peak temperature of Indium with a sample mass of 1 mg and a heating rate of 10 °C/min. It is the aim to generate a correction factor for the extrapolated and/or peak temperature when the sample mass and the heating rate are given. A chosen heating rate and an acceptable maximal temperature deviation induce a recommended sample mass. Analogous, a chosen sample mass and an acceptable maximal temperature deviation induce a recommended heating rate.

The experimental data of the extrapolated onset temperatures have been fitted using the following 'black box' formula:

$$T_{EO}(S_h, m) = a_0 + a_1 m + a_2 m^2 + (b_0 + b_1 m + b_2 m^2) S_h + (c_0 + c_1 m + c_2 m^2) S_h^2 \quad (5)$$

with $T_{EO}(S_h, m)$: extrapolated onset temperature, dependent on the sample mass and the heating rate (°C); S_h: heating rate (°C/min); m: sample mass (mg); $a_0 = 156.415$; $a_1 = 0.00667531$; $a_2 = -0.000215105$; $b_0 = 0.0160736$; $b_1 = 0.00240142$; $b_2 = -0.000227395$; $c_0 = -1.34755 \times 10^{-5}$; $c_1 = 5.20908 \times 10^{-7}$; $c_2 = 6.16263 \times 10^{-8}$.

The residues are smaller than or equal to the experimental errors put in. Fig. 4a shows the fittings of the experimental data. As before, using (2), the fit fails for the combination of low sample mass (0.113 mg) and high heating rates (>100 °C/min). This is related to the findings mentioned before: in this region the limits of the apparatus are encountered.

In a similar way, multivariate linear regression-analysis has been used to fit the peak temperature values of Indium with various masses and different heating rates:

$$T_P(S_h, m) = a'_0 + a'_1 \log_{10} m + \{b_0 + b'_1 \log_{10} m + (b'_2 \log_{10} m)^2\} \sqrt{S_h + c'_0 + c'_1 \log_{10} m} \quad (6)$$

with $T_P(S_h, m)$: peak temperature, dependent on the sample mass and the heating rate (°C); S_h: heating rate (°C/min); m: sample mass (mg); $a'_0 = 154.384$; $a'_1 = 0.682398$; $b'_0 = 0.606787$; $b'_1 = 0.22259$; $b'_2 = 0.140185$; $c'_0 = 18.1224$; $c'_1 = -13.3221$.

The residues are smaller than or equal to the experimental errors put in. Fig. 4b represents the experimental data, and the fitting by the proposed formula. As can be seen, the peak temperature values are fitted well.

The proposed formulas, (5) and (6), are used to calculate the correction factor both for the extrapolated onset and for the peak temperatures, respectively, which are dependent on the sample mass and the heating rate.

The correction factor for the extrapolated onset is defined as

$$CF_{T,EO} = T_{EO,ref} - T_{EO}(S_h, m) \quad (7)$$

with $T_{EO,ref} = 156.6$ °C for the primary standard Indium of 1 mg and heated at 10 °C/min.

Table 3 represents the matrix of the correction factor for the extrapolated onset calculated by applying formula (7), as based on the fittings by (5). These values can be used to correct for the thermal lag of the extrapolated onset of an HPer DSC measurement where a sample with a certain mass, m, has been scanned at a chosen heating rate, S_h. The correction factors at heating rates of 100 °C/min and higher are rounded off to unity (shaded area in Table 3) because an experimental error of 1 °C has been taken into account.

The correction factor for the peak temperature is defined as

$$CF_{T,P} = T_{P,ref} - T_P(S_h, m) \quad (8)$$

with $T_{P,ref} = 157.6$ °C for the primary standard Indium of 1 mg and heated at 10 °C/min (one has to recline that this peak (extremum) value is instrument specific!).

In analogy to Tables 3 and 4, represents the matrix of the correction factors for the peak temperature calculated by applying formula (8), as based on fittings using (6).

In principal, by using these formulas and the resulting correction factors, the procedure sketched should result, at least in the heating mode, to correct temperatures of certain phase transitions, for the HPer DSC used. When applying the right correction factor(s), one is able to compare in a proper way the transition temperatures of a particular sample measured at different heating rates. In practice Tables 3 and 4 provide useful guidelines for optimal experimental conditions. It is recommended to *design* the experiments in this way, instead of just applying corrections afterwards.

3.2. Temperature calibration in the cooling mode

Surely for heat-flux calorimeters (mostly large furnaces) and possibly also for power-compensation calorimeters (small furnaces) one would expect asymmetry of the heat transfer with respect to heating and cooling. Höhne et al. reported their work concerning the calibration of thermal analysis instruments in the cooling mode [18]. They suggested, based on experimental results performed with liquid crystals, that for the same low scanning rate, the heating and cooling thermal lags were symmetrical. A useful guideline for temperature, heat and heat flow rate calibration of scanning calorimeters in the cooling method was published by Sarge et al. [5]. They proposed the use of the same procedures in the cooling mode as to those applied in the heating mode. Liquid crystals and substances with higher-order phase transitions are recommended for temperature calibration

Table 3
Matrix of the correction factor for the extrapolated onset calculated by using formula (7), as based on fitting using (5)

S_h (°C/min)	Correction factor for the extrapolated onset: $CF_{T,EO}$ (°C)								
	Sample mass (mg)								
	0.5	1	2	3	4	5	6	7	8
1	+0.2	+0.2	+0.2	+0.1	+0.1	+0.1	+0.1	+0.1	+0.1
5	+0.1	+0.1	+0.1	+0.1	+0.1	0.0	0.0	0.0	0.0
10	0.0	0.0	0.0	0.0	−0.1	−0.1	−0.1	−0.1	−0.1
20	−0.2	−0.2	−0.2	−0.3	−0.3	−0.3	−0.3	−0.3	−0.3
30	−0.3	−0.4	−0.4	−0.5	−0.5	−0.5	−0.5	−0.5	−0.5
40	−0.5	−0.5	−0.6	−0.7	−0.7	−0.7	−0.7	−0.7	−0.7
50	−0.6	−0.7	−0.8	−0.9	−0.9	−0.9	−0.9	−0.9	−0.9
100	−1	−2	−2	−2	−2	−2	−2	−2	−2
150	−2	−2	−3	−3	−3	−3	−3	−3	−3
200	−3	−3	−3	−4	−4	−4	−4	−4	−4
250	−3	−4	−4	−4	−5	−5	−5	−5	−5
300	−4	−4	−5	−5	−6	−6	−6	−6	−6
400	−5	−5	−6	−7	−7	−7	−7	−7	−7
500	−5	−6	−7	−8	−8	−9	−9	−9	−9

because of the absence of supercooling during cooling, in contrast with the general occurrence of supercooling for first-order phase transitions. Menczel and Leslie suggested a procedure for performing DSC calibrations on cooling [19]. In their procedure they made use of liquid crystalline transitions of high-purity liquid crystals. A number of possible compounds to apply for calibration of DSCs in the cooling mode were investigated by Hakvoort et al. [8,16]. Recently, work has been published [20] concerning the evaluation of the calibration errors on cooling of a power-compensation differential scanning calorimeter using different sets of standard metals. Alternative, physically meaningful procedures for carrying out the calibration on cooling are analyzed and validated. The authors mention that any pair of standard materials may be used to calibrate on cooling and that the calibration errors increase for wider working temperature ranges.

The obvious route for calibrating the HPer DSC at different cooling rates would be to use the fitting approach used for Indium during heating. To verify this postulate the HPer DSC has to be examined on its symmetry and whether any deviations found are acceptable. If however, the results of the calibration obtained in the cooling mode are too different from those in the heating mode, the HPer DSC is asymmetrical to heating and cooling. Such asymmetry would arise if the heat transfer in cooling is appreciably different from the heat transfer in heating. As a result, different heat flow rates would be operative during heating and cooling, leading to different temperature calibration factors. Therefore it is necessary to check the symmetry starting from the calibration performed in the heating mode as discussed before. For this relative calibration, it is sufficient to use pure substances whose transitions do not tend to supercool, if possible, or show only a small and well-defined supercooling.

Table 4
Matrix of the correction factor for the peak temperature calculated by using formula (8), as based on fittings using (6)

S_h (°C/min)	Correction factor for the peak temperature: $CF_{T,P}$ (°C)								
	Sample mass (mg)								
	0.5	1	2	3	4	5	6	7	8
1	+0.8	+0.6	+0.4	+0.3	+0.3	+0.3	+0.3	+0.4	+0.4
5	+0.6	+0.3	+0.1	0.0	−0.1	−0.1	−0.1	−0.1	−0.1
10	+0.4	0.0	−0.3	−0.5	−0.5	−0.6	−0.7	−0.7	−0.7
20	−0.1	−0.5	−0.9	−1.2	−1.3	−1.4	−1.5	−1.6	−1.6
30	−0.5	−1.0	−1.5	−1.7	−1.9	−2.1	−2.2	−2.3	−2.3
40	−0.8	−1.4	−2.0	−2.3	−2.5	−2.7	−2.8	−2.9	−3.0
50	−1.2	−1.8	−2.4	−2.7	−3.0	−3.2	−3.3	−3.5	−3.6
100	−3	−3	−4	−5	−5	−5	−6	−6	−6
150	−4	−5	−6	−6	−7	−7	−7	−7	−8
200	−5	−6	−7	−8	−8	−8	−9	−9	−9
250	−6	−7	−8	−9	−9	−10	−10	−10	−11
300	−6	−8	−9	−10	−10	−11	−11	−12	−12
400	−8	−9	−11	−12	−12	−13	−13	−14	−14
500	−9	−11	−12	−13	−14	−15	−15	−16	−16

Table 5
Results of the temperature calibration both in heating and cooling mode of some secondary reference materials

Substance (transition)	S (°C/min)	T_P (°C)		T_{EP} (°C)[a]	$T_{EP} - T_{P,ref}$ (°C)[b]	Supercooling = $(T_{P,h} - T_{P,c})$ (°C)[c]
		150	5	0	0	0
M24 (S–N)	Heating	[d]	67.2	67.1	0	0.1
	Cooling	62.1	66.9	67.0	−0.1	
HP-53 (S–N)	Heating	122.4	120.3	120.2	0	0.0
	Cooling	115.0	120.1	120.2	0	
BCH-52 (N–L)	Heating	168.6	165.3	165.2	0.4	0.1
	Cooling	160.8	165.0	165.1	0.3	

[a] T_{EP} values in this column are the extrapolated peak temperatures measured at scan rates of 50 °C/min and lower towards a scan rate of 0 °C/min.
[b] T_{EP}: peak temperatures after extrapolation to scan rate 0 °C/min. $T_{P,ref}$ equals the T_P reference values, which are represented in Table 1.
[c] $T_{P,h}$ and $T_{P,c}$ are the extrapolated (towards a scan rate of 0 °C/min) peak temperature values, respectively, in heating and cooling.
[d] No result can be obtained due to overlapping of the first transition peak (crystalline–smectic) with the requested transition temperature (smectic–nematic).

For temperature calibration of differential scanning calorimeters in both heating and cooling modes, secondary calibration standards have been used as reference materials. Sarge et al. [5] (see also http://www.gefta.uni-freiburg.de) recommended substances for temperature calibration in the cooling mode. Three secondary calibration substances, i.e. 4-cyano-4′-octyloxybiphenyl (M24), 4-(4-pentyl-cyclohexyl)-benzoic acid-4-propyl-phenyl ester (HP-53) and 4′-ethyl-4-(4-propyl-cyclohexyl)-biphenyl (BCH-52), were selected and their phase transition temperatures are presented in Table 1. M24, HP-53 and BCH-52 are secondary reference materials for testing the accuracy of DSC's according to ISO 9001. They are traceable to standard reference materials from NIST,[1] (SRM 2222 - Biphenyl) and PTB[2] (ZRM 31402 - In, ZRM 31403 - Sn). HPer DSC measurements on M24, HP-53 and BCH-52 (having sample masses in between 0.9 and 1.1 mg) were performed both for various cooling (from 5 to 300 °C/min) and heating (from 5 until 300 °C/min) rates.

For M24, three different phase transition peak temperatures around 55 (crystalline–smectic; CS), 67.1 (smectic–nematic; SN) and 80.2 °C (nematic–isotropic; NI) can be distinguished using standard heating rates. These phase transitions shift gradually to higher temperature values with increasing heating rates and to lower temperature values with increasing cooling rates as can be seen in Fig. 9a. The smectic–nematic transition is recommended by NIST to use for DSC calibration.

In a same way, for HP-53, HPer DSC measurements distinguish three different phase transition peak temperatures around 73, 93.6 and 120.5 °C (only two transitions are seen in cooling in this study; Fig. 9b). The smectic–nematic transition at 120.5 °C is recommended by NIST to use for DSC calibration.

For BCH-52, Fig. 9c shows two different phase transition temperatures at around 149 and 164.8 °C; at 10 °C/min. The nematic–liquid transition at 164.8 °C is recommended by NIST to use for DSC calibration. All the peak temperatures of these various phase transitions were determined after extrapolation to scan rate 0 °C/min, T_{EP}, of the peak maximum in both heating and cooling modes. The literature and measured values of the smectic–nematic (for M24 and HP-53) and nematic–liquid (for BCH-52) phase transitions are represented in Table 5. Supercoolings as low as 0.1 °C for M24; 0 °C for HP-53 and 0.1 °C for BCH-52 have been found, in agreement with the certification of the batch, which reports supercoolings of 0–0.2 °C in the cooling mode. The curves concerning the peak temperature versus heating and cooling rate of M24, HP-53 and BCH-52 (Fig. 9) suggest symmetry for the heating and cooling modes. Thus, for this HPer DSC and for the selected sample masses the same relations with respect to heating and cooling rates are observed. In addition, as mentioned for M24, HP-53 and BCH-52 the points of intersection at 0 °C/min for the cooling and heating behavior coincide within an interval of <0.1 °C. Thus, as conclusion, it is evident that a separate calibration in the cooling mode is not necessary for the HPer DSC instrument used by us.

In order to decide whether the proposed correction factors of Indium as based on heating can be used in the cooling mode too, the melting behavior of Indium and the secondary standards have to be compared. Therefore, the behavior of the extrapolated onset and the peak temperatures of the secondary standards, measured with different heating rates, are compared with those of the primary calibration standard Indium, all with a comparable sample mass. Fig. 10a shows the comparison of the extrapolated onset and the peak temperatures of HP-53, BCH-52 and Indium as function of the heating rate. The extrapolated onset temperature of M24 is not presented, because it is impossible to determine these values undisputed at heating rates up to 300 °C/min. No large differences between the evolution of the heating behavior of secondary standards and that of Indium are seen. The ΔT values, which are the differences between the peak and the extrapolated onset temperatures, of HP-53, BCH-52 and Indium as function of the square root of the heating rate are shown in Fig. 10b. For ΔT, a maximal difference of about 1 °C is found between the calibrants. Compared to Indium, HP-53 and BCH-52 show even lower ΔTs. Obviously, the results obtained, shown in Fig. 10, show clear resemblance between Indium and HP-53 and BCH-52.

Because the heating behavior of these calibration standards are similar to Indium for different rates, the formulas (5–8) can be used to correct for the sample mass and scanning rates in

[1] NIST: National Institute of Standards und Technology, Gaithersburg, USA.
[2] PTB: Physikalisch—Technische Bundesanstalt, Braunschweig, Germany.

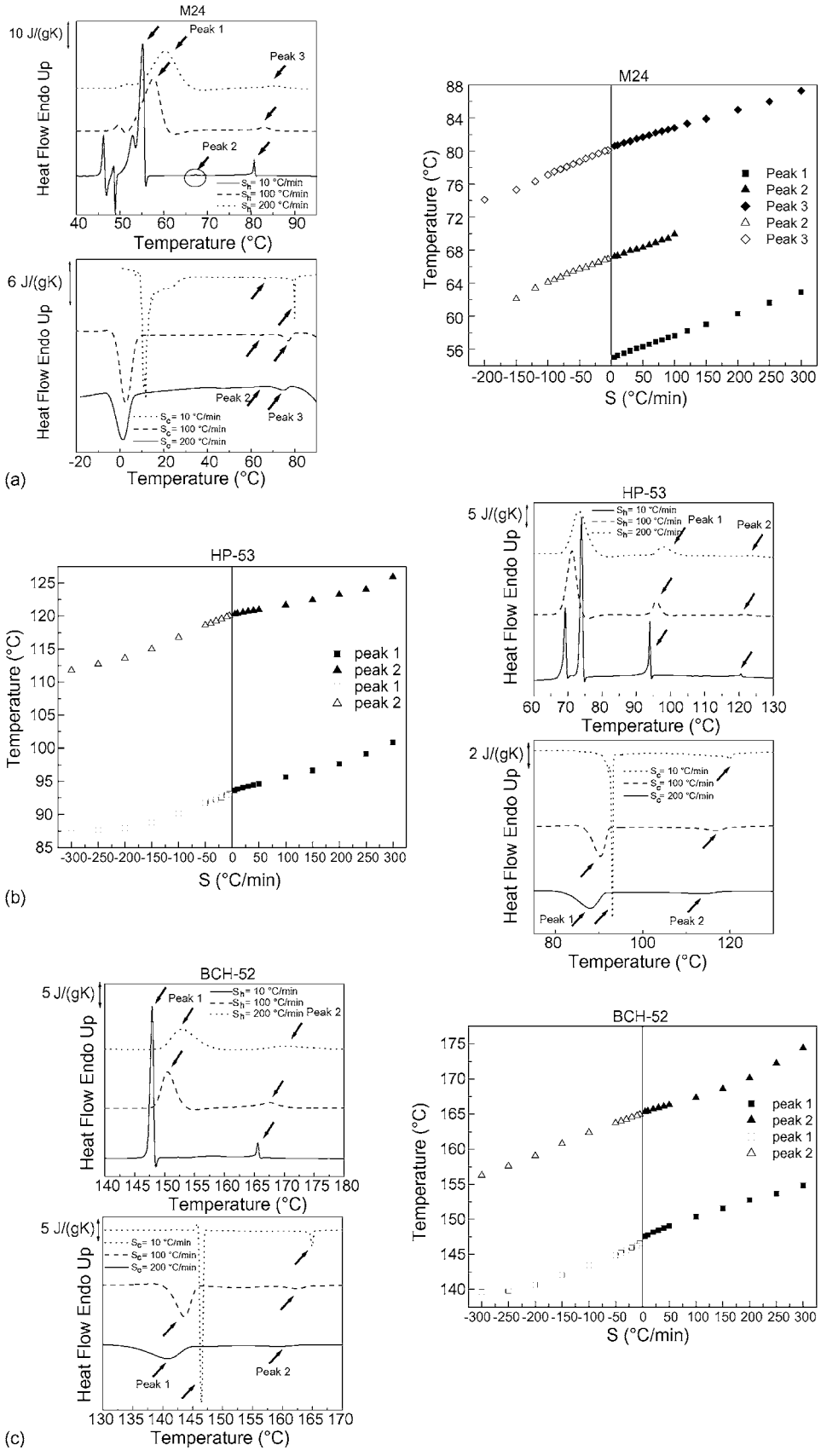

Fig. 9. HPer DSC curves in the heating and cooling mode (S = 10, 100 and 200 °C/min) representing the peak temperatures of the phase transitions of (a) M24, (b) HP-53 and (c) BCH-52 as a function of the cooling and heating rate. All samples have a sample mass in between 0.9 and 1.1 mg.

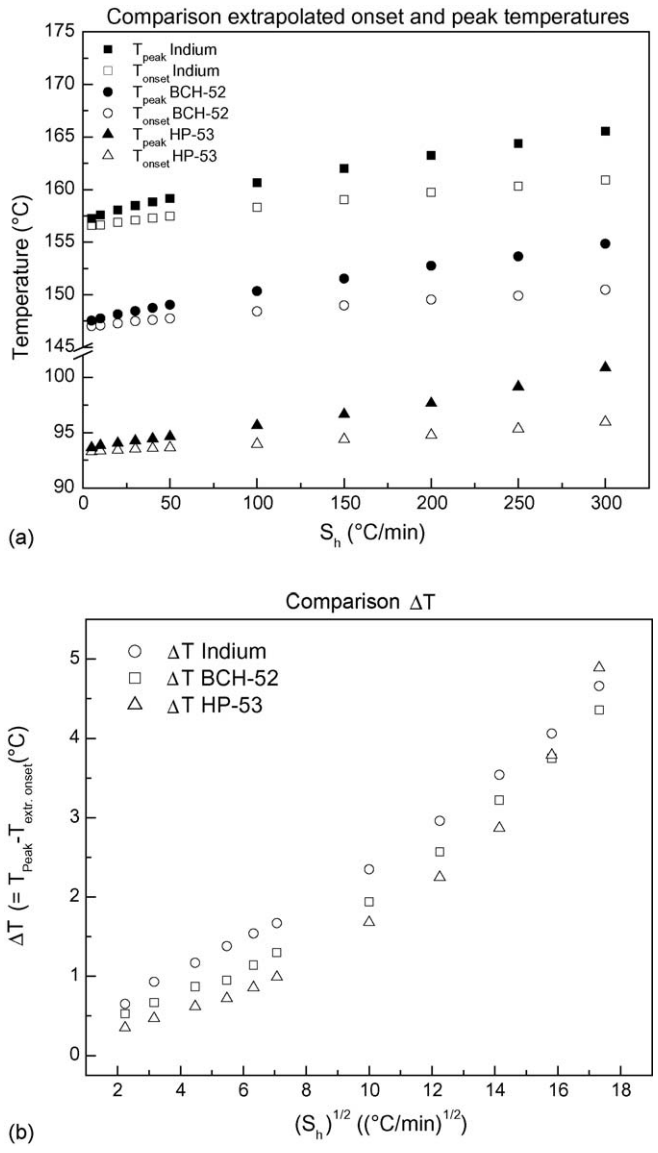

Fig. 10. Comparison of the melting behavior of the secondary standards BCH-52 and HP-53 with Indium, with equivalent sample masses (1 ± 0.1 mg) and for different heating rates. (a) Comparison of the extrapolated onset and peak temperatures as a function of the heating rate and (b) comparison of ΔT values as a function of the square root of the heating rate.

both heating and cooling modes. The symmetry found leads to the advantage that the temperature calibration could be carried out in the heating and cooling mode with only a few experiments, or even just in the heating mode.

If the cooling behavior deviates more than accepted (this might be arbitrary) with respect to the heating behavior, a similar matrix for the cooling mode like the one for the heating mode of Indium has to be constructed by way of experiments on a secondary standard with various sample masses and different cooling rates. In an analogous way also, matching constants of the proposed formulas (5–8) have to be calculated. Thus, asymmetry of the HPer DSC furnaces with respect to heating and cooling would unfortunately lead to rather time consuming calibrations.

The authors of this article emphasize the importance of a calibration of HPer DSCs and other calorimeters for both sample masses and heating and cooling rates. It facilitates making the right choices with respect to these parameters beforehand (at the start of measurements), instead of making corrections afterwards. Anyhow, all efforts should be directed towards minimizing of the thermal lag, besides realization of a proper temperature calibration.

4. Conclusions

In this article temperature calibration of scanning calorimeters in the heating and the cooling mode for various sample masses and various scan rates is discussed. Besides primary calibration standards like Indium, usable for calibration in heating, three secondary calibration standards, M24, HP-53 and BCH-52, were studied and found to be suitable for calibration in the cooling mode.

Finally, recommendations are postulated concerning the temperature calibration of scanning calorimeters in both heating and cooling modes and minimization of thermal lag.

4.1. Recommended procedure for temperature calibration of scanning calorimeters in the heating and the cooling mode for various sample masses and various scan rates

(a) Perform a normal temperature calibration with primary standards (1 mg) in the relevant temperature range at 10 °C/min heating.
(b) Measure the extrapolated onset and peak temperatures of Indium with different sample masses and various heating rates. Fit these experimental results with the two proposed formulas (5–8) and determine the correction factors with respect to 1 mg of Indium at a heating rate of 10 °C/min. Construct two calibration matrices similar to those in Tables 3 and 4: one for the extrapolated onset and another for the peak temperature.
(c) Check the symmetry of the scanning calorimeter, using, e.g. the calibration standards in Table 5 and according to the procedure discussed in the text.
  - *Symmetry* means it is possible to use the same formulas describing the Indium correction factors for the calibration in heating also in the cooling mode.
  - *Asymmetry* means a construction of a new calibration matrix in the cooling mode by using one of the mentioned secondary standards (M24, HP-53 or BCH-52).

4.2. Simplified procedure for temperature calibration of scanning calorimeters in the heating and the cooling mode for one sample mass and various scan rates

In order to simplify the extensive calibration of HPer DSC, one specific sample mass has to be chosen (preferably 1 mg).

If the symmetry of the HPer DSC with respect to the cooling and the heating mode is checked and found to be good:

(a) Perform a normal calibration with primary standards (1 mg) in the relevant temperature range.

(b) Measure the extrapolated onset and peak temperatures of Indium with one particular mass (1 mg) and various heating rates. Construct two calibration lines: one for the extrapolated onset and another for the peak temperature. These calibration lines can likewise be used in the cooling mode.

If the symmetry of the HPer DSC with respect to the cooling and the heating modes is checked and found to be poor:

(a) Perform a normal calibration with primary standards (1 mg) in the relevant temperature range.
(b) Measure the extrapolated onset and peak temperatures of one of the secondary standards, M24, HP-53 or BCH-52 with a sample mass of 1 mg and various heating and cooling rates. Construct four calibration lines: two concerning the extrapolated onset in the heating and cooling mode, and two concerning the peak temperatures in the heating and cooling mode.

Acknowledgements

This work was performed in the framework of a European Union Marie Curie Industry Host Fellowship of Geert Vanden Poel: contract No. HPMI-CT-2002-00180. All measurements were performed at DSM Research in The Netherlands. The authors appreciate the contribution of Tom Hillegers of the Mathematical and Statistical group of DSM Research, and the discussions with Thijs Pijpers, Katholieke Universiteit Leuven, België.

References

[1] T.F.J. Pijpers, V.B.F. Mathot, B. Goderis, R.L. Scherrenberg, E. van der Vegte, High-speed calorimetry for the study of the kinetics of (de)vitrification, crystallization, and melting of macromolecules, Macromolecules 32 (2002) 3601–3613.
[2] S.C. Mraw, D.F. Naas, The measurement of accurate heat capacities by differential scanning calorimetry. Comparison of d. s. c. results on pyrite with literature values from precision adiabatic calorimetry, J. Chem. Thermodyn. 11 (1979) 567–584.
[3] Å. Fransson, G. Bäckström, Automated differential scanning calorimetry at low temperatures, Int. J. Thermophys. 6 (1985) 165–175.
[4] G.W.H. Höhne, H.K. Cammenga, W. Eysel, E. Gmelin, W. Hemminger, The temperature calibration of scanning calorimeters, Thermochim. Acta 160 (1990) 1–12.
[5] S.M. Sarge, G.W.H. Höhne, H.K. Cammenga, W. Eysel, E. Gmelin, Temperature, heat and heat flow rate calibration of scanning calorimeters in the cooling mode, Termochim. Acta 361 (2000) 1–20.
[6] S.-S. Chang, E.F. Westrum Jr., Heat capacities and thermodynamic properties of globular molecules. I. Adamantane and hexamethylentetramine, J. Phys. Chem. 64 (1960) 1547–1551.
[7] E.F. Westrum Jr., The thermophysical properties of three globular molecules, J. Phys. Chem. Solids 18 (1961) 83–85.
[8] G. Hakvoort, C.M. Hol, DSC investigation of some testing and some calibration compounds particulary during cooling, J. Therm. Anal. Cal. 52 (1998) 195–202.
[9] P.J. van Ekeren, C.M. Hol, A.J. Witteveen, A comparative test of differential calorimeters, J. Therm. Anal. 49 (1997) 1105–1114.
[10] G. Hakvoort, C.M. Hol, DSC calibration during cooling, J. Therm. Anal. Cal. 56 (1999) 717–722.
[11] S.M. Sarge, E. Gmelin, G.W.H. Höhne, H.K. Cammenga, W. Hemminger, W. Eysel, The caloric calibration of scanning calorimeters, Themochim. Acta 247 (1994) 129–168.
[12] F. Grønvold, Heat capacity and thermodynamic properties of metallic tin in the range 300 to 1000 K. Fusion characteristics, Rev. Chim. Min. 11 (1974) 568–584.
[13] S.M. Sarge, W. Hemminger, E. Gmelin, G.W.H. Höhne, H.K. Cammenga, W. Eysel, Metrologically based procedures for the temperature, heat and heat flow rate calibration of DSC, J. Therm. Anal. 49 (1997) 1125–1134.
[14] E.B. Amitin, Yu.F. Mimenkov, O.A. Nabutovskaya, I.E. Paukov, S.I. Sokolova, Thermodynamic properties of gallium from 5 to 320 K, J. Chem. Thermodyn. 16 (1984) 431–436.
[15] F. Grønvold, Enthalpy of fusion and temperature of fusion of indium and redetermination of the enthalpy of fusion of tin, J. Chem. Thermodyn. 25 (1993) 1133–1144.
[16] G. Hakvoort, C.M. Hol, P.J. van Ekeren, DSC calibration during cooling. A survey of possible compounds, J. Therm. Anal. 64 (2001) 367–375.
[17] K.H. Illers, Die ermittlung des schmelzpunktes von kristallinen polymeren mittels wärmeflusskalorimetrie (DSC), Eur. Polym. J. 10 (1974) 911–916.
[18] G.W.H. Höhne, W. Hemminger, H.-J. Flammersheim, Differential Scanning Calorimetry, An Introduction for Practitioners, Springer-Verlag, Berlin, 1996.
[19] J.D. Menczel, T.M. Leslie, Temperature calibration of an electrical compensation DSC on cooling using thermally stable high purity liquid crystals, J. Therm. Anal. 40 (1993) 957–970.
[20] M.J.A. Malheiro, J.A. Martins, J.J.C. Cruz Pinto, Evaluation of the calibration errors on cooling of a differential scanning calorimeter using different sets of standard metals, Thermochim. Acta 420 (2004) 155–161.